Naval Research Laboratory
Washington, DC 20375-5320

SHIM-Fire Breadboard Instrument Design, Integration, and First Measurements

CHRISTOPH R. ENGLERT
J. TIMOTHY BAYS

Upper Atmospheric Physics Branch
Space Science Division

JEFFREY C. OWRUTSKY

Chemical Dynamics and Diagnostics Branch
Chemistry Division

JOHN M. HARLANDER

St. Cloud State University
St. Cloud, Minnesota

November 23, 2005

REPORT DOCUMENTATION PAGE

Public reporting burden for this collection of information is estimated to average 1 hour per response, including the time for reviewing instructions, searching existing data sources, gathering and maintaining the data needed, and completing and reviewing this collection of information. Send comments regarding this burden estimate or any other aspect of this collection of information, including suggestions for reducing this burden to Department of Defense, Washington Headquarters Services, Directorate for Information Operations and Reports (0704-0188), 1215 Jefferson Davis Highway, Suite 1204, Arlington, VA 22202-4302. Respondents should be aware that notwithstanding any other provision of law, no person shall be subject to any penalty for failing to comply with a collection of information if it does not display a currently valid OMB control number. **PLEASE DO NOT RETURN YOUR FORM TO THE ABOVE ADDRESS.**

1. REPORT DATE *(DD-MM-YYYY)* 23-11-2005	2. REPORT TYPE Memorandum Report	3. DATES COVERED *(From - To)* February 2005 - July 2005

4. TITLE AND SUBTITLE

SHIM-Fire Breadboard Instrument Design, Integration, and First Measurements

5a. CONTRACT NUMBER

5b. GRANT NUMBER

5c. PROGRAM ELEMENT NUMBER

6. AUTHOR(S)

Christoph R. Englert, John M. Harlander,* Jeffrey C. Owrutsky, and J. Timothy Bays**

5d. PROJECT NUMBER

5e. TASK NUMBER

5f. WORK UNIT NUMBER

7. PERFORMING ORGANIZATION NAME(S) AND ADDRESS(ES)

Naval Research Laboratory
4555 Overlook Avenue, SW
Washington, DC 20375-5320

8. PERFORMING ORGANIZATION REPORT NUMBER

NRL/MR/7640--05-8926

9. SPONSORING / MONITORING AGENCY NAME(S) AND ADDRESS(ES)

Office of Naval Research
800 North Quincy Street
Arlington, VA 22217

10. SPONSOR / MONITOR'S ACRONYM(S)

11. SPONSOR / MONITOR'S REPORT NUMBER(S)

12. DISTRIBUTION / AVAILABILITY STATEMENT

Approved for public release; distribution is unlimited.

13. SUPPLEMENTARY NOTES

*St. Cloud State University, St. Cloud, MN
**USNR, NR ONR S&T HQ 100

14. ABSTRACT

This report covers the design, integration, characterization, and the first test measurements of the Spatial Heterodyne Imager for Fire (SHIM-Fire) breadboard instrument. The main objective of SHIM-Fire is to explore the method of hyperspectral fire detection in the near infrared (NIR). It is intended as a more sophisticated and improved method for fire detection compared to the long wavelength video detection (LWVD) approach, which has already been developed within the VS program. One of the goals of SHIM-Fire is to utilize the combination of spectral and spatial resolution inherent to hyperspectral imaging to achieve better nuisance rejection than LWVD.

15. SUBJECT TERMS

Fire detection; Optical fire detector; Spatial heterodyne spectroscopy

16. SECURITY CLASSIFICATION OF:			17. LIMITATION OF ABSTRACT	18. NUMBER OF PAGES	19a. NAME OF RESPONSIBLE PERSON Christoph R. Englert
a. REPORT Unclassified	b. ABSTRACT Unclassified	c. THIS PAGE Unclassified	UL	22	19b. TELEPHONE NUMBER *(include area code)* (202) 767-5528

Standard Form 298 (Rev. 8-98)
Prescribed by ANSI Std. Z39.18

Contents

SHIM-Fire Breadboard
(Spatial Heterodyne Imager for Fire – Breadboard)
Instrument Design, Integration and First
Measurements

1. Introduction and Background

This report covers the design, integration, characterization, and the first test measurements of the SHIM-Fire (Spatial Heterodyne Imager for Fire) breadboard instrument. This effort was part of the Spectral-based component of the Volume Sensor (VS) program, which is part of the Advanced Damage Countermeasures (ADC) Future Naval Capabilities (FNC) program. The main objective of SHIM-Fire is to explore the method of hyperspectral fire detection in the near infrared (NIR). It is intended as a more sophisticated and improved method for fire detection compared to the long wavelength video detection (LWVD) approach, which has already been developed within the VS program. One of the goals of SHIM-Fire is to utilize the combination of spectral and spatial resolution inherent to hyperspectral imaging to achieve better nuisance rejection than LWVD.

The following sections provide background information about the VS and LWVD programs and the technique of Spatial Heterodyne Spectroscopy (SHS).

1.1. Volume Sensor Program and Long Wave Video Detection

The primary objective of the Volume Sensor Program is to use optical as well as acoustic detection methods for inexpensive, remote and real-time monitoring of ship spaces, including the detection of fire and smoke. One goal is to achieve faster response times without increasing the false alarm rate compared to those typical of point detection sensors (e.g., of heat, smoke, or gases, such as CO or CO_2), which depend on molecular or thermal diffusion from the fire or smoke source to the sensor. Optical and acoustic sensors do not rely on diffusion, so they can provide stand-off detection and possibly faster response times to more quickly identify a fire or other hazardous conditions.

The central element of the VS approach is the identification of fire, smoke, and other conditions using video image detection (VID) systems in which the images are analyzed by machine vision algorithms. The capability has been implemented using commercial VID systems, [Gottuk et al. 2004; Rose-Pehrsson et al. 2004a] which are quite effective at identifying smoke and direct line of sight (LOS) fires. VID systems can respond quickly but typically require a direct LOS between the source and detector for effective detection of flame or fire. This is a drawback of VID systems since it is not feasible for practical or economical reasons to deploy enough sensors to ensure complete direct LOS coverage throughout the compartment space, especially in crowded spaces that are typical of Navy ships. Long wavelength video detection has been developed in the VS Program as a method to complement the VID systems [Steinhurst et al. 2003; Owrutsky and Steinhurst 2005]. LWVD uses standard (silicon-based CCD) cameras and a long pass

filter (LPF). The idea is to use the LPF to suppress the visible image and thus enhance the sensitivity for reflected emission from fires and hot objects. LWVD has been demonstrated to provide effective detection of reflected flames emission for sources outside the field of view of the sensors or camera, thereby significantly reducing the number of cameras required to monitor a cluttered space for fires. In addition, other kinds of sensors are being incorporated into the VS system as described elsewhere [Rose-Pehrsson et al. 2004b; Steinhurst et al. 2003]. The LWVD is one component of the multisensor, data fusion-based VS system that has been developed at NRL and characterized in a series of full scale fire tests carried out aboard the ex-USS Shadwell.

LWVD was developed in the Spectral-based component of Volume Sensor (SBVS), in which various approaches to optical fire and smoke detection were investigated using methods that involve monitoring emitted radiation outside the visible region of the spectrum. It is important that the multisensor detection system developed in the VS program be inexpensive yet effective. Therefore, within the SBVS, it did not seem feasible to implement a method that yielded both spectrally and spatially resolved information, so that two separate approaches were pursued. One employed several narrow band single element sensors operating at various wavelengths from the ultraviolet to the mid infrared. This technique is similar to commercially available flame detectors. It utilizes spectral resolution without any imaging. The other method, LWVD, provides imaging without any detailed spectral information. In order to minimize the cost, near infrared imaging or LWVD was implemented because it can use commonly available, inexpensive cameras. These can be simple surveillence cameras (for <$100) or commercial cameras (i.e., camcorder for <$1000), both of which cost much less than mid infrared cameras (3-12 microns, >>$5000). Although mid infrared cameras outperform LWVD, the latter provides a desirable trade off between cost and performance for the applications described here. SHIM-Fire represents an effort to simultaneously achieve both spatial and spectral information for fire detection.

Long wavelength (LW) or near infrared emission radiation detectors have been used before for fire detection [Zhu et al. 1998; Lloyd et al. 1998; Sivathanu et al. 2000]. These reports and patents represent approaches intended to detect reflected NIR emission using several narrow band detectors without any imaging capability. The results demonstrated the feasibility of detecting reflected NIR emission. In addition, NIR video detection has been investigated for fire detection in cargo bays [Sentenac et al. 2002; Chan and Burge 1999]. The study by Sentenac et al. [2002] includes a detailed characterization of using CCD cameras operating in the NIR for remote temperature measurement and demonstrated a minimum detectable temperature of about 350° C.

In our LWVD approach to fire detection, we use a long pass filter (LPF) positioned in front of a camera that has a standard CCD array. The LPF transmits light with wavelengths longer than a cutoff, typically between 700 and 900 nm, which increases the contrast for fire, flame, and hot objects by suppressing the normal, visible video images of the space. This provides modest thermal imaging. There is more emission from hot objects in this spectral region than in the visible (<600 nm). LW videos are beneficial for providing high contrast and therefore straightforward LOS detection for flames and hot objects (including bulkheads heated by obstructed fires), and for identifying obstructed fire and flame based on reflected light. Currently, the LWVD system is analyzed with a straightforward luminosity algorithm, in which the integrated brightness over the image is

monitored and a threshold above the previously determined background is used as the alarm criteria. While LWVD is quite sensitive and effective for detecting reflected emission from sources outside the field of view of the camera, it is also susceptible to false alarms from nuisance sources. It will alarm on a variety of sources that increase the light level in the NIR. As a result, in the data fusion and VS system algorithm, a system alarm requires more than just an LWVD system alarm; it must be accompanied by an alarm from either the VID or spectral sensor systems. There are currently efforts to develop more discriminating image analysis routines to better distinguish real fires from nuisance sources so that the LWVD can operate more effectively as a stand alone system. But another approach is to achieve more information in the video data collection. This is the motivation for exploring the use of SHS as an improvement over regular LWVD. The hope is that spatially and spectrally encoded video achievable with hyperspectral imaging using instruments like SHIM-Fire will result in better discrimination between real and nuisance sources.

## 1.2. *Spatial Heterodyne Spectroscopy*

Spatial Heterodyne Spectroscopy is a relatively novel optical technique. It was developed in the late 1980s at the University of Wisconsin for ultraviolet remote sensing. The basic concept of SHS is described in detail in publications by Harlander et al. [1992, 1994, 2003]. The concept is similar to a Michelson interferometer with the return mirrors replaced by fixed, tilted diffraction gratings. Figure 1 shows the basic SHS concept.

Some important properties of SHS are:
- SHS has no moving parts and can be built in a very rugged, compact package.
- SHS has interferometric throughput like Fourier transform spectrometers (FTS) and can be fieldwidened with fixed prisms. Thus, SHS instruments typically allow for higher throughput than grating spectrographs, especially at high spectral resolution.
- In contrast to conventional FTS which record the interferogram in the time domain, SHS interferometers allow the simultaneous detection of all path differences with an imaging detector. This makes it a "single shot" technique, like a conventional grating spectrometer. This property is particularly important if the scene is rapidly changing during a measurement (like a flame), which has the potential to contaminate an FTS interferogram.
- In SHS, the maximum bandwidth is limited by the combination of the number of detector array elements in one dimension and the resolving power.
- Like FTS, SHS is subject to multiplex noise, which compared to a grating spectrometer with equal throughput results in a signal to noise ratio (S/N) disadvantage. However, especially for high spectral resolution, SHS has a throughput advantage, that can be used to compensate or overcompensate this effect to achieve an equal or higher S/N.

In the past, SHS has mainly been applied in the ultraviolet spectral region, where SHS allows the design of very high spectral resolution and high throughput instruments that are particularly small and rugged. NRL's Space Science Division has built a proof of

3

concept UV SHS instrument [Harlander et al. 2002; Cardon et al. 2003] for middle atmospheric remote sensing which was flown on the Space Shuttle in 2002. An improved version of SHIMMER (Spatial Heterodyne Imager for Mesospheric Radicals) [Harlander et al. 2003] is scheduled to be launched in late 2006 as the primary payload of STPSat-1, a DoD Space Test Program mission.
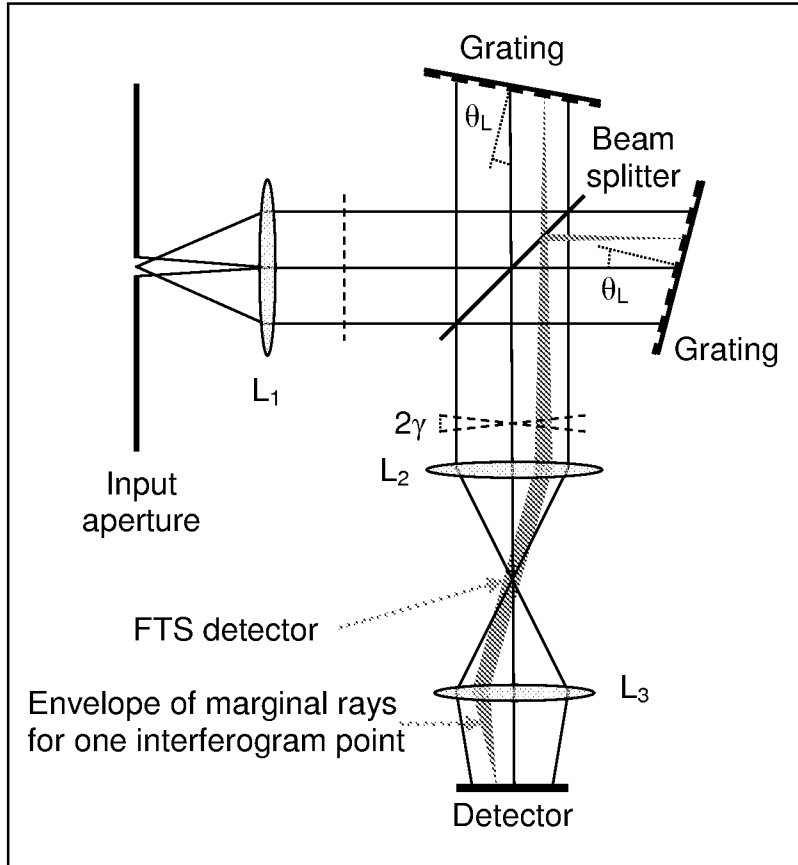
Figure 1: *Basic SHS concept. A plane wavefront (dashed line) is divided into the two interferometer arms by a beamsplitter. The two arms are terminated by fixed, angled diffraction gratings that tilt the wavefronts with respect to the optical axis. The tilt angle is proportional to the heterodyned wavenumber of the signal (σ-σ_0), where σ_0 is the Littrow wavenumber of the gratings which is determined by the grating grove density and grating angle. The tilted wavefronts are recombined at the beamsplitter and form Fizeau fringes at the detector array. In this example, the wavefronts are crossed in the middle, which yields a double sided interferogram with zero path difference in the middle and increasing path differences towards the edges of the array. (Figure from: Englert et al. [2004])*

The ability to observe a changing scene without using moving parts and the ability to simultaneously provide one dimensional spatial information and spectral information makes SHS a candidate for the investigation of hyperspectral fire detection, which motivated this project.

In the following sections we present the initial requirements of the breadboard instrument, the final optical design and integration (including a complete parts list), the measurements of key properties of the spectrometer, and the first measurements.

2. Optical Design and Instrument Integration

The design goals for this breadboard instruments were initially specified as:

Bandpass: ~700 nm -1100 nm
Spectral resolution: < 4 nm
Spatial resolution: ~ 10 field of view slices

The overall scope of the design effort was a simple, moderate spectral resolution, NIR SHS instrument that uses a 2 dimensional imaging detector for simultaneous spectral and one dimensional spatial observations. Figure 2 illustrates this observational concept.
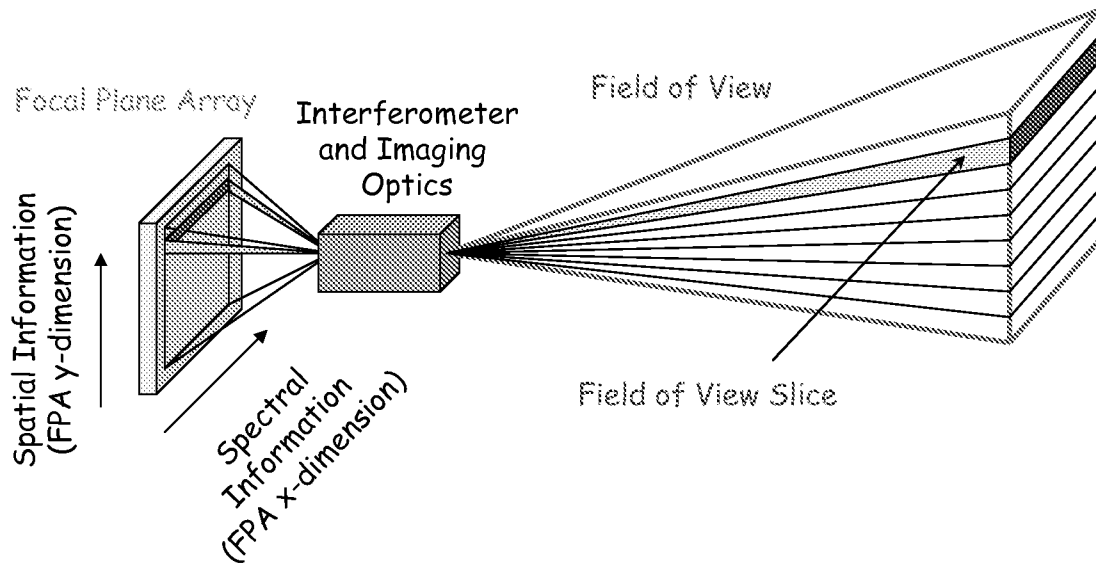
Figure 2: *Imaging scheme of the SHIM-Fire breadboard. Every slice in the field of view produces an interferogram along a row of the detector. For this instrument, the focal plane array (FPA) is binned into 10 slices, which yields 10 interferograms/spectra per exposure.*

For this effort, commercial off the shelf (COTS) items were used to the greatest extent possible. No sensitivity requirements were established, but a best effort was be made to optimize all parameters within the scope of this project. Table 1 contains a complete COTS parts list of the breadboard instrument. Only a small number of custom parts were used to facilitate the mounting of several optical components. The only other custom part is the instrument cover.

Table 1: List of all COTS parts

	Parts List	
	Item	**Quantity**
1	Newport Plano Convex Cylindrical Lens CKX050 AR.16 (f=50.2mm)	2
2	Newport Plano Concave Lens KPC028 AR.16 (f=200mm)	1
3	Newport ID-1.0 iris	1
4	Newport Bi Convex Lens KBX052 AR.16 (f=50.2mm)	1
5	Edmund NT47-012 beamsplitter	1
6	Newport 53004BK01-129R, 60 g/mm grating	2
7	Edmund NT45-338 mirror	1
8	Edmund NT54-754 filter IR (Hoya R-72)	1
9	Edmund NT54-798 telecentric lens 0.5X mag	1
10	MicroPix M-640 monochrome CCD camera	1
11	Newport MRL-12M mini optical rail	1
12	Newport MCC mini rail carrier	4
13	Newport LH-1 lens mount	4
14	Newport MFM-B bracket	3
15	Newport MFM-075 optical mount	3
16	Newport 423 translation stage	2
17	Newport SM-25 actuator	2
18	Edmund NT56-025 mounting clamp	1
19	Newport SA-12, 12" X 24" solid aluminum plate (optical bench)	1

2.1. Anamorphic Telescope

The purpose of the anamorphic telescope is to image the observed scene in one dimension onto the gratings, while completely defocusing the other dimension. That is, a point source in the field of view results in a line image on the grating, perpendicular to the grating groves. This line image is then imaged onto the detector, so that each point source creates a complete interferogram. This also means that the source structure in each slice of the scene (see Figure 2) is completely washed out at the detector and therefore does not contaminate the spectral information contained in the interferogram.
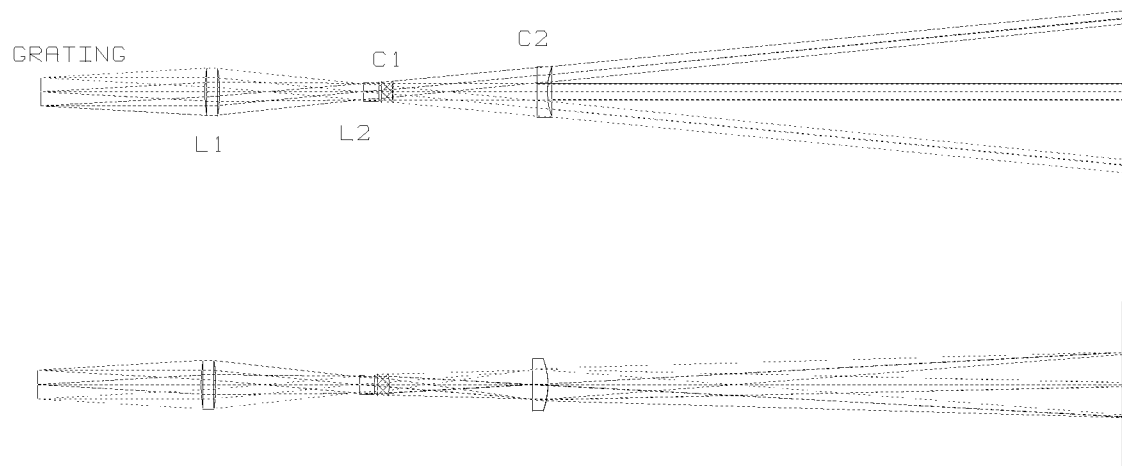
Figure 3: *Telescope design. Top panel: Parallel to grating groves. Bottom panel: Perpendicular to grating grooves.*

The telescope for this breadboard instrument contains two plano convex-cylindrical lenses (C1, C2, part#1), a biconvex lens (L1, part#4), and a plano concave lens (L2, part#2) as shown in Figure 3. An iris is placed between L1 and L2, right at L2.

The alignment of the telescope was accomplished by placing the iris one focal length away from L1, placing L2 immediately in front of the iris, changing the position of both lenses and the iris with respect to the grating until an object at ~1 meter distance was imaged on the grating, placing C1 as close to L2 as possible, and placing C2 so that a point source at object distance forms a narrow line at the grating.

Moving the first cylinder lens (C2) results in a change in the object distance. A raytracing model calculation using the as built distances of the lenses results in the following separations of the two cylinder lenses for a variety of object distances:

| Object Distance	C1-C2 Center to Center Distance
100 mm	57.3 mm
200 mm	27.0 mm
400 mm	17.5 mm
1000 mm	13.0 mm
2000 mm	11.6 mm

The telescope is shown on the left side of Figure 4. All other COTS parts used for the telescope, e.g. holders, rail etc., are included in the parts list (Table 1). The lens material is BK7 for all telescope lenses.

2.2. Interferometer

The interferometer consists of two COTS gratings (part#6) and a COTS beamsplitter (part#5). It is shown on the top left of Figure 4 and in Figure 5.
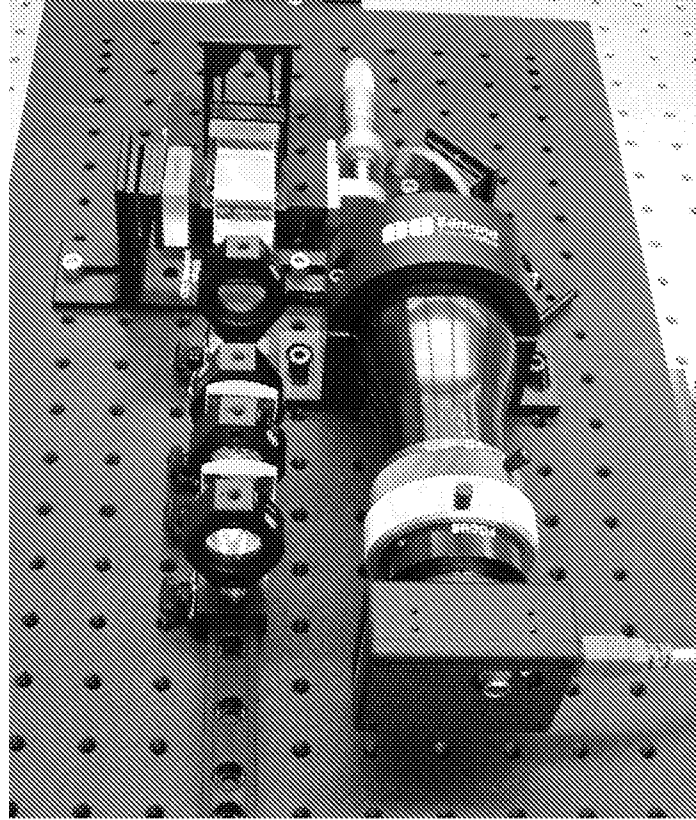
Figure 4: *Optical lay out of the breadboard instrument.*
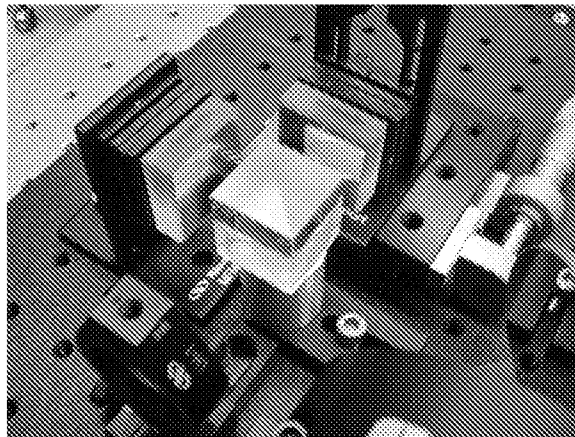
Figure 5: *SHIM-Fire interferometer. The light enters from the left. Both gratings are mounted on 3 point, adjustable mounts. One grating can be translated using a micrometer driven translation stage.*

The plane ruled reflectance gratings[1] are blazed for 750nm (1.26°) and have a groove density of 60 mm^{-1}. The gratings are mounted using 3 point optical mounts (part #15) which allow for easy adjustment of the grating angles. The output grating can be translated along the optical axis using a translation stage (Part #16/17). The translation of one grating causes the zero path distance location, the location where the gratings "cross", to move in the dimension perpendicular to the grating grooves.

The nonpolarizing, BK7 cube beamsplitter[2] has a metallic/dielectric hybrid coating. For SHS instruments, cube or hexagonal beamsplitters are preferred over uncompensated plate beamsplitters because they minimize the wavelength dependent phase shift (chirping) in the measured interferogram.

The rough alignment of the interferometer was performed using a visible (red) laser diode. The final adjustment was accomplished using an NIR laser diode.

2.3. Exit Optics

The beam exiting the interferometer is first folded by 90° to keep the design compact. The fold mirror (part#7) is gold coated for optimum reflectance in the NIR. It is mounted on a 3 point lens mount (part #15) for easy adjustment just like the gratings. Following the mirror and mounted to the entrance aperture of the imaging lens is a NIR long pass filter (part#8). The filter transmittance (R-72) is shown in Figure 6 together with the wavelength response of the FPA. The combination of these two curves limits the sensitivity of this instrument to about 700 nm – 900 nm.
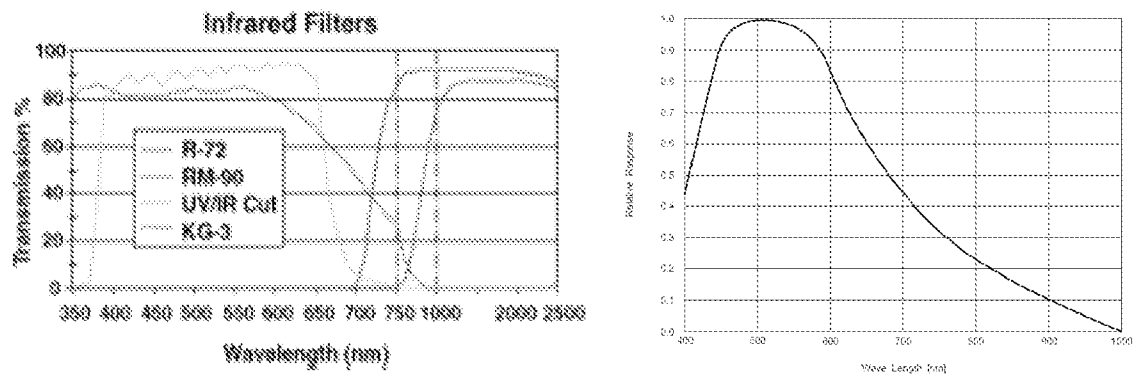
Figure 6: *Left Panel: R-72 Filter transmittance[3]. Right Panel: Sensitivity of the Focal Plane Array[4]. The combination of the filter transmittance and the FPA sensitivity effectively forms a bandpass filter (~700 nm – 900 nm) for this instrument.*

The imaging optics used to image the gratings (fringe localization plane) onto the camera focal plane array is a COTS telecentric lens[5] (part#9) with a primary

[1] http://gratings.newport.com/products/efficiency/effFrame.asp?sku=010l53-*-129R
[2] http://www.edmundoptics.com/onlinecatalog/displayproduct.cfm?productID=2239
[3] http://www.edmundoptics.com/onlinecatalog/displayproduct.cfm?productid=1524
[4] http://www.datasheetcatalog.com/datasheets_pdf/I/C/X/0/ICX084AL.shtml
[5] http://www.edmundoptics.com/onlinecatalog/displayproduct.cfm?productID=1630

magnification of 0.5. This telecentric lens includes a focus adjustment and an internal, adjustable iris. This lens was chosen for this instrument because it is easy to adjust and it provides appropriate imaging quality. In addition, telecentric lenses have the advantage that the magnification does not change with the focus adjustment. The iris within the telecentric lens can be used to reject higher order light from the gratings.

2.4. Detector array

The focal plane array (FPA) is a Sony ICX-084AL integrated into the Micopix M-640 camera package[6]. The FPA has 640x480 usable pixels and the camera is oriented so that the 640 pixels are in the dispersion plane so that the measured interferograms have 640 samples. The camera has an IEEE-1394 compliant Firewire interface.

The long wavelength cut off is limited by the detector sensitivity. Moving the long wavelength cutoff further into the red would require an infrared enhanced silicon FPA or a different detector material, like Gallium Arsenide (GaAs).

The window that is placed in front of the FPA was removed to avoid fringing and/or additional absorption of the NIR signal. The camera is directly mounted onto the telecentric lens using the C/CS mount.

For the first measurements presented in this report, the control software that is part of the camera package was used in combination with simple IDL (Research Systems Inc.) code to read the data and perform further processing. A custom control software package tailored to the SHS application is currently under development.

3. Characterization

3.1. Field of View

The field of view (FOV) can be determined by scanning a localized source (like a small flashlight) through the focal plane of the telescope. The initial FOV measurement resulted in a FOV of approximately $12.7° \times 5.4°$ (vertical × horizontal). The vertical FOV is divided/binned into 10 slices by the software, so that each slice contains 48 rows of the FPA. Figure 7 shows a typical image with a light source illuminating one slice of the FOV.

A different telescope that expands the FOV from 12.7° to about 60° will be implemented for future test measurements of SHIM-Fire. A wider FOV in the vertical (imaging) dimension is anticipated to simplify the coverage of a larger volume like a room or ship compartment.

---

[6] http://www.ccddirect.com/store/pdf/micropix.pdf
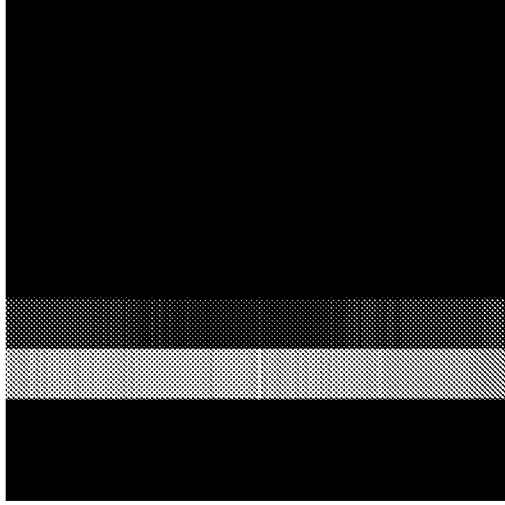
Figure 7: *Binned, raw FPA data. This image shows the interferogram of a flashlight in one of the 10 slices of the FOV. The brightest vertical line in the middle of the interferogram is the zero path difference location. The remainder of the interferogram has very low contrast due to the broadband spectrum of the incandescent light bulb.*

3.2. Frequency Calibration

The easiest way to perform a frequency calibration is to use two known spectral features like two lines in an emission spectrum. We have used a neon lamp for this purpose. Using the measured fringe frequency (f_1 & f_2) of two emission lines and their known line positions (λ_1 & λ_2) one can calculate the wavelengths corresponding to each spatial frequency $\lambda(f)$, assuming a small grating angle Θ_L, as shown in the following example:

$\lambda_1 = 724.517$ nm $\qquad\qquad$ $f_1 = 37.5$ fringes / array width
$\lambda_2 = 837.761$ nm $\qquad\qquad$ $f_2 = 194.5$ fringes / array width

Littrow wavelength:

$$\lambda_0 = \frac{f_2 - f_1}{(f_2 / \lambda_1) - (f_1 / \lambda_2)} = 701.9 \; nm$$

Grating angle:

$$\Theta_L = \arcsin\left(\frac{\lambda_0 * 60 \cdot 10^{-6} nm^{-1}}{2}\right) = 1.206°, \text{ where } 60 \cdot 10^{-6} \text{ nm}^{-1} \text{ is the grating groove density}$$

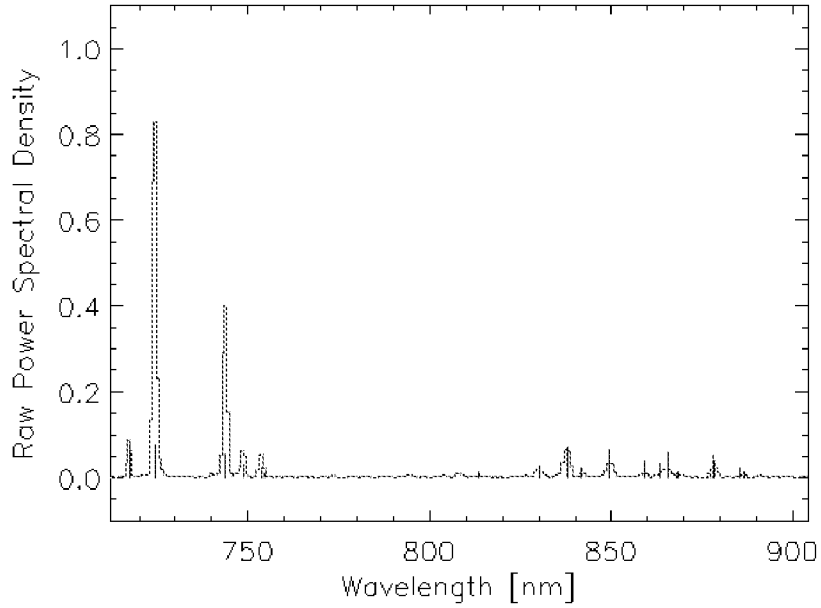Length of the grating imaged on the FPA:

$$w = \frac{f_1}{4\left(1/\lambda_0 - 1/\lambda_1\right)\tan(\Theta_L)} = 0.999 \; cm$$

Wavelength as a function of spatial frequency:

$$\lambda(f) = \frac{\lambda_0}{1 - \dfrac{f}{2 \cdot 600\ cm^{-1} \cdot w}}$$, where 600 cm^{-1} is the grating groove density

Figure 8 shows the measured Ne spectrum registered to the proper wavelength grid.

Figure 8: *Spectrum recorded using a Ne pencil style calibration lamp. The interferogram was apodized with a Hanning function prior to the transformation into the spectral domain. The blue lines indicate the theoretical line positions and relative intensities [Martin et al. 1999].*

An image of a ruler positioned right at the input grating taken with the same exit optics and FPA confirms the imaged grating width of about 1cm (shown in Figure 9).
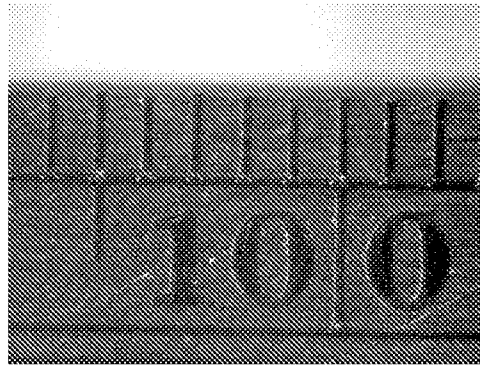

Figure 9: *Picture of a ruler positioned in front of a grating. The scale is 1 division per millimeter, confirming that the imaged grating width is about 1cm.*

12

3.3. Instrumental Line Shape and Resolving Power

The theoretical resolving power is equal to the number of imaged grating grooves on both gratings. For this instrument, the maximum resolving power is $\lambda/\Delta\lambda = 2 \cdot 0.999$ cm $\cdot$ 600 cm^{-1} ≈ 1199 which is equivalent to 0.67 nm at 800 nm. Note that the actual resolution of the instrument is slightly smaller than that due to apodization of the interferogram caused by the finite aperture. Any post processing apodization to reduce the ringing in the instrumental line shape function (ILS) will result in a further reduction of the resolution, similar to FTS.

A simple verification of the ILS of the breadboard instrument was performed using the monochromatic signal from an NIR laser diode, diffused behind the iris in the telescope. Figure 10 shows a typical interferogram in the upper panel and the ILS obtained after zero filling and phase correcting [Englert et al. 2004] the interferogram. The characteristic sinc (sin(x)/x) shape familiar from FTS is clearly visible. The gray trace in the lower panel shows the difference between the measured ILS and a perfect sinc.
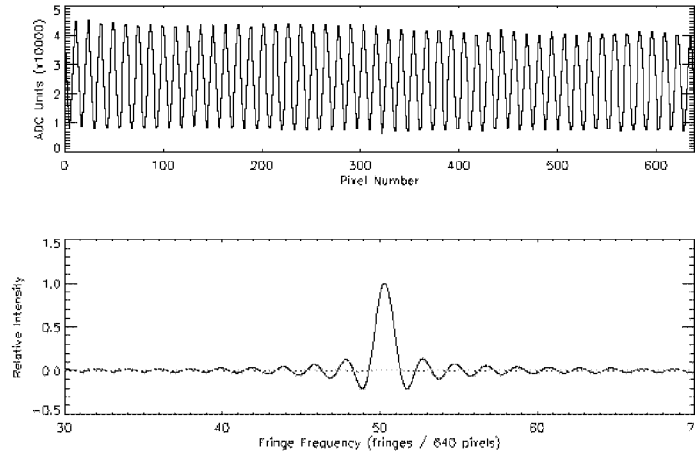

Figure 10: *Upper Panel: Interferogram of an NIR laser diode. No dark or flatfield correction applied. Lower Panel: Spectrum retrieved from the interferogram in the upper panel after zero filling and phase correction. The ringing is caused by the finite length of the interferogram as it is familiar from FTS. The gray trace is the difference between the retrieved spectrum and a sinc function.*

3.4. Spectral Response

Generally, the shape of the spectral response can be measured using a source with known spectral density. We did not have such a source available but used a broadband, spectrally flat source (an incandescent AA MagLite) to qualitatively assess the spectral response. Figure 11 shows the spectrum measured using the MagLite. The spectral density of the MagLite is not constant between 700 nm and 900 nm. The color temperature of the light bulb is expected to be higher than 2500 K which means that the spectral density (Watt/cm^2/cm^{-1}/steradian) increases with wavelength by up to a factor of 3 within the

passband. The qualitative shape of the measured response is as expected. The sharp cut off at 700 nm is due to the long pass filter, while the slow decline in response for longer wavelengths can be attributed to the decreasing sensitivity of the FPA (see Figure 6).
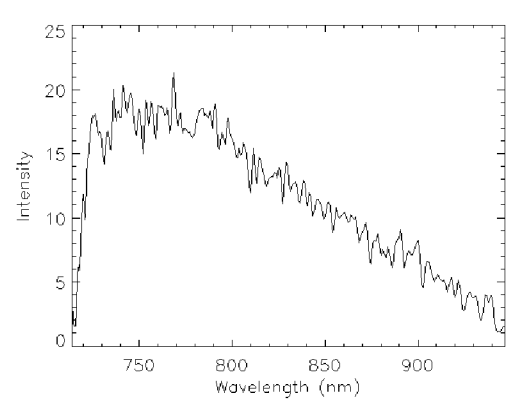
Figure 11: *Dark field corrected spectrum of an iridescent MagLite. The qualitative shape of this broadband spectrum is as expected: A steep decline in response near 700 nm due to the spectral filter and a slow decline toward longer wavelengths due to the decreasing sensitivity of the FPA.*

The spectrum in Figure 11 is only corrected for dark current. The measurement is an average of 44 exposures with a total integration time of 0.132 seconds. The structure in the spectrum is caused by statistical noise and flatfield effects [Englert et al. 2005] which have not been taken into account.

4. First Laboratory Fire Measurements

4.1. Data

First laboratory fire measurements were conducted by pointing the FOV of the instrument at small flames in a fume hood. These measurements were acquired using the software package provided with the camera and simple IDL codes to store the data and convert measured interferograms into power spectra in real time. The flames typically filled one to three slices of the field of view.

The main objectives of these measurements were to operate the instrument in a test environment and to learn what features the new instrument control software should include. A secondary goal was to investigate any spectral features present in the data for different flames, like atomic or molecular lines or variations in the spectral shape of the thermal background. The fires observed included NaF, I_2, and KCl dissolved in methyl alcohol and isooctane, as well as wood, cotton, nylon, high density polyethylene, high density Styrofoam, a propane torch, and Teflon in the flame of a propane torch.

The IDL code provided power spectra in real time with a measurement frequency of about one exposure every 3 seconds. No dark, phase, or flatfield correction was applied.

14

The resulting power spectra can be divided into four major groups:

- Very bright potassium (K) lines
- K lines and broad thermal background
- K lines and corresponding ghosts
- Only broad thermal background
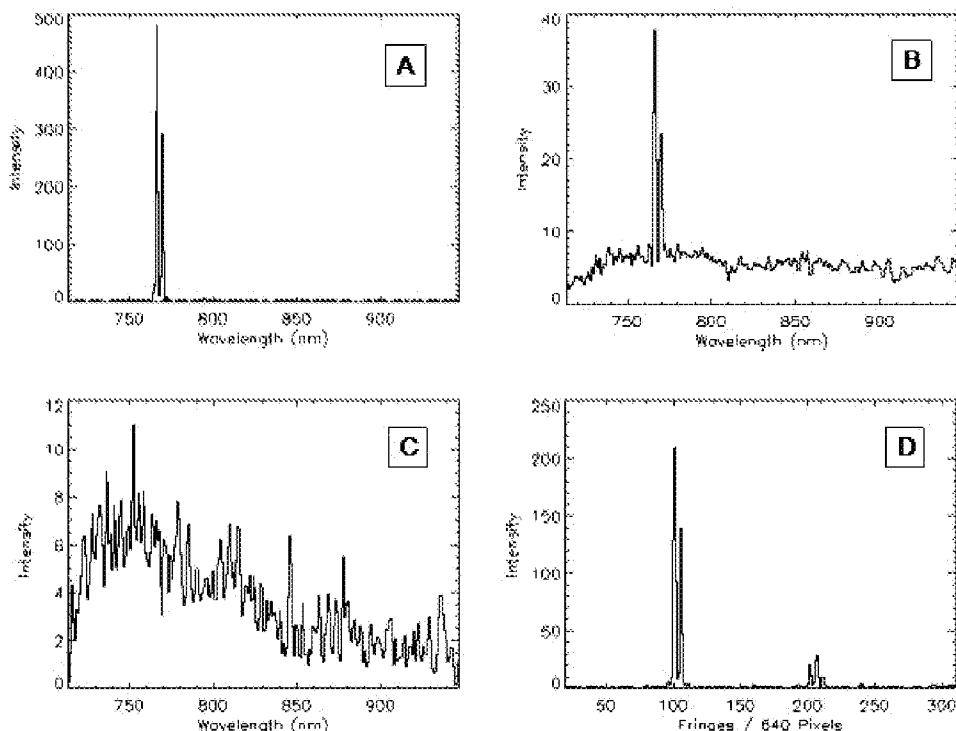
Figure 12: *A: KCl in methanol. This spectrum shows the two strong K emission lines at 766.4911 nm and 769.8974 nm [Martin et al. 1999]. The lines are so strong that the spectrally broad thermal background is not visible on this scale. B: High density Styrofoam. The spectrum shows the K lines, but the lines are much weaker, so that the thermal background is clearly visible. C: Wood match in isopropanol. This is a very dim signal dominated by the thermal background and systematic dark current and flatfield features. D: KMnO$_4$ in isopropanol. This spectrum shows the K lines and ghosts of the K lines at twice the fringe frequency. The presence of ghosts is due to the saturation of pixels in the detector array, which essentially clips the interferogram at the high signal values.*

Figure 12 shows examples for each of these groups of spectra. All spectra are power spectra, no dark, phase, or flatfield correction was applied. The interferograms were apodized using a Hanning function.

Other than the potassium lines, no further atomic or molecular lines could be identified in the spectra of the different flames. Differences in the shape of the spectrally broad thermal backgrounds like shown in Figure 12 B & C were observed.

15

4.2. Conclusions and Recommendations

We have successfully designed, integrated, characterized, and tested an SHS breadboard instrument for the NIR (~720-900 nm) with the resolving power of ~0.7 nm (~1.4 nm when using interferogram apodization with a Hanning function). The instrument provides spatial resolution in one dimension (10 segments) and all interferogram samples are recorded simultaneously, so that a changing scene does not contaminate the recovered spectral information.

The first fire measurements using the breadboard instrument lead to a number of conclusions and recommendations concerning the instrument control software and user interface:

- The control software that was delivered with the camera includes an auto exposure time feature. This function is generally desirable for scenes that change their brightness within a large dynamic range, like a developing fire. However, it presents a problem when viewing a scene that flickers because the time constant of the exposure time adjustment is short, i.e. in the range of the inverse flicker frequency. We recommend exploring an auto exposure time algorithm with a longer time constant and saturation protection for the future instrument control software developments. All stored, saturated (over exposed) exposures shall be marked as such.
- New control software should enable real time data acquisition at a rate higher than one exposure every three seconds.
- New control software should make it easier to start and stop measurements with and without saving the measured data.
- Real time data analysis should include at least a dark current correction. A flatfield correction is desirable, as well as phase correction to lower the systematic and random noise in the spectrum.

The conclusions from the spectral data gathered during this first test involving small fires in a fume hood are:

- Many of the flames showed the two strong K lines around 768 nm. The lines are so strong that even small contaminations of the burning substance with potassium cause the lines to be visible.
- Any other atomic or molecular emission features, if at all present, were too weak to be detected at the S/N of these measurements.
- The observed differences between the spectrally broad thermal backgrounds can most likely be attributed to differences in flame temperature. A more detailed investigation of the thermal background as a function of fuel, flame temperature, and reflected/scattered versus direct flame observations could be the objective of a future test.

16

Acknowledgements

References

Cardon J.G., C.R. Englert, J.M. Harlander, F.L. Roesler M.H. Stevens, "SHIMMER on STS-112: Development and Proof-of-Concept Flight," AIAA Paper: 2003-6224, AIAA Space 2003 - Conference & Exposition, Long Beach, CA, Sept. 23-25, 2003.

Chan, W.S., and J.W. Burge, "Imaging flame detection system," United States Patent 5,937,077, August 10, 1999.

Englert, C.R., J.M. Harlander, J.G. Cardon, F.L. Roesler, "Correction of Phase Distortion in Spatial Heterodyne Spectroscopy," Applied Optics, **43**, 6680-6687, 2004.

Englert, C.R., Harlander J.M., "Flatfielding in Spatial Heterodyne Spectroscopy," submitted to Applied Optics, 2005.

Gottuk, D.T., J.A. Lynch, S.L. Rose-Pehrsson, J.C. Owrutsky, F.W. Williams, "Video Image Fire Detection for Shipboard Use," AUBE 2004, Duisburg, Germany, September 14-16, 2004.

Harlander J.M., R.J. Reynolds, and F.L. Roesler, "Spatial heterodyne spectroscopy for the exploration of diffuse interstellar emission lines at far ultraviolet wavelengths," Astrophysical Journal, **396**, 730-740, 1992.

Harlander J.M., H.T. Tran, F.L. Roesler, K.P. Jaehnig, S.M. Seo, W.T. Sanders, and R.J. Reynolds, "Field-Widened Spatial Heterodyne Spectroscopy: Correcting for Optical Defects and New Vacuum Ultraviolet Performance Tests," in *EUV, X-Ray and Gamma-Ray Instrumentation of Astronomy V*, O.E. Siegmund and J. Vallerga, eds., Proc. SPIE 2280, 310-319, 1994.

Harlander J.M., F.L. Roesler, J.G. Cardon, C.R. Englert, and R.R. Conway, "SHIMMER: A Spatial Heterodyne Spectrometer for Remote Sensing of Earth's Middle Atmosphere," Applied Optics, 41, 1343-1352, 2002.

Harlander J.M., F.L. Roesler, C.R. Englert, J.G. Cardon, R.R. Conway, C.M. Brown, J. Wimperis, "Robust monolithic ultraviolet interferometer for the SHIMMER instrument on STPSat-1," Applied Optics, 42, 2829-2834, 2003.

Lloyd A.C., Y.J. Zhu, L.K. Tseng, J.P. Gore, and Y.R. Sivanthanu, "Fire Detection Using reflected Near Infrared Radiation and Source Temperature Discrimination," NIST GCR 98: 747, 1998.

Martin, W.C., J.R. Fuhr, D.E. Kelleher, A. Musgrove, L. Podobedova, J. Reader, E.B. Saloman, C.J. Sansonetti, W.L. Wiese, P.J. Mohr, and K. Olsen, "NIST Atomic Spectra Database (version 2.0, 1999)," http://physics.nist.gov/asd, 1999.

Owrutsky, J.C., and D.A. Steinhurst, "Fire Detection Method," Patent Application Number 2005/0012626, January 20, 2005.

Rose-Pehrsson, S.L., J.C. Owrutsky, S.C. Wales, F.W. Williams, J.P. Farley, D.A. Steinhurst, C.P. Minor, J.A. Lynch, D.T. Gottuk, "Volume Sensor for Damage Assessment and Situational Awareness," AUBE 2004, Duisburg, Germany, September 14-16, 2004a.

Rose-Pehrsson, S.L., J.C. Owrutsky, D.T. Gottuk, D.A. Steinhurst, C.P. Minor, J.P. Farley, F.W. Williams, "Volume Sensor for Shipboard Damage Control," 2004 NRL Review, p. 144, 2004b.

Sentenac, T., Y. Le Maoult, and J.-J. Orteu, "Evaluation of a charge-coupled-device-based video sensor for aircraft cargo surveillance," Optical Engineering 41, 796-810, 2002.

Sivathanu, Y., R.K. Joseph, L. Tseng, J.P. Gore, and A. Lloyd, "Flame and Smoke Detector," United States Patent 6,111,511, August 29, 2000.

Steinhurst, D.A., C.P. Minor, J.C. Owrutsky, S.L. Rose-Pehrsson, D.T. Gottuk, F.W. Williams, and J.P. Farley, "Long Wavelength Video-based Event Detection, Preliminary Results from the CVNX and VS1 Test Series, ex-USS *Shadwell*, April 7-25, 2003," Naval Research Laboratory Memorandum Report NRL/MR-MM/6110—03-8733, December 31, 2003.

Zhu Y.-J., A. Lloyd, Y. Sivathanu, and J. Gore, "Experimental and Numerical Evaluation of a Near Infrared Fire Detector," Fire Research and Engineering Second (2nd) International Conference (ICFRE2), Slaughter KC, Editor, p. 512, 1998.